Delft University of Technology

Joint Performance Optimization of Monostatic and Bistatic SAR Configurations

Onat, Nehir Berk ; Dogan, Ozan; Azcuetac, Mario ; Sloun, Ruud van

Important note
To cite this publication, please use the final published version (if applicable).
Please check the document version above.

JOINT PERFORMANCE OPTIMIZATION OF MONOSTATIC AND BISTATIC SAR CONFIGURATIONS

Nehir Berk Onat[a,c], Ozan Dogan[b], Mario Azcueta[c], Ruud van Sloun[a]

[a] Eindhoven University of Technology, The Netherlands
[b] Delft University of Technology, The Netherlands
[c] MetaSensing B.V., The Netherlands

ABSTRACT

This study focuses on the optimization of phased array antenna excitation coefficients for a spaceborne synthetic aperture radar (SAR) system, comprising a joint monostatic and bistatic configuration. An amplitude-only binary-coded Genetic algorithm (BGA) is proposed for the joint non-linear optimization problem to improve monostatic and bistatic SAR performance metrics. Based on the developed optimizer, significant performance improvement is achieved for both configurations.

Index Terms— Bistatic SAR, Beam Forming, Genetic Algorithm, Optimization.

1. INTRODUCTION

Since many years, spaceborne synthetic aperture radar (SAR) has been providing high-resolution images to reveal the unique features on Earth's surface that may not be obtained by an optical sensor. SAR imaging system can be monostatic, comprising a single platform with transmitter and receiver, bistatic or multistatic which can be divided into fully and semi-active configurations [1]. Specifically, bistatic spaceborne SAR imaging has started to draw attention due to its potential applications like high resolution wide swath imaging[2], tomography, single pass interferometry, and others [3].

SAR imaging performance is heavily dependent on the SAR antenna radiation pattern characteristics. The key performance parameters of SAR systems that quantify undesired affects involve noise equivalent sigma zero (NESZ), range ambiguity to signal ratio (RASR) and azimuth ambiguity to signal ratio (AASR) [4]. Imaging performance can be optimized with respect to these performance parameters by an adequate selection of the phased array excitation coefficients.

In recent years, many algorithms were implemented to optimize the monostatic antenna pattern. The problem of planar array synthesis has a very large solution space, and finding a global optimum solution from this space can be very challenging for deterministic optimization methods [5]. Additionally, these methods heavily rely on accurate a-priori information

Parameter	Value
Sensor altitude	627 [km]
Velocity of the satellite	7633 [m/s]
Along track baseline	10 [km]
RF center frequency	1.275 [GHz]
Chirp bandwidth	22 [MHz]
Doppler bandwidth	1873 [Hz]
PRF	2173 [Hz]
Slant range (MS)	773 - 805 [km]
Off-nadir angle (MS)	34.2 - 36.2°
Incident angle (MS)	30.1 - 41.3°
Resolution (δ_{az} x δ_{gr})	5 [m] x 10 [m]
Antenna height x length (MS)	3.47 [m] x 9.97 [m]
Number of elements el x az (MS)	20 x 7
Antenna height x length (CS)	1.10 [m] x 2.92 [m]
Number of elements el x az (CS)	6 x 16

Table 1. Main system parameters for the considered swath

tion in order to converge to a minimum. Stochastic global optimization methods, such as Genetic algorithm (GA), do not require initial conditions and tend to converge to the global optimum [6]. Furthermore, the bistatic measurement performance is discussed in [7] without a beam forming optimization. However, to the best of our knowledge, none of these methods consider the pattern optimization problem for both a monostatic and bistatic configuration operating concurrently.

In this work, we focus on the joint performance optimization of a monostatic and bistatic SAR imaging system that comprises an active master satellite (MS) with a small and passive companion satellite (CS) flying in close-formation. Section 2 discusses the reference scenario. The main SAR performance parameters comprising the cost function of the optimizer are presented in the following section. In Section 4, the implemented optimizer, binary-coded Genetic algorithm (BGA), is demonstrated. Results and conclusions are drawn in the succeeding sections.

2. SYSTEM SETUP

The parameters of the MS and CS are based on the Argentina's L-band system SAOCOM, that operates as monostatic, and the European Space Agency (ESA) that operates as receive-only companion satellite (SAOCOM-CS) [8, 9]. Both satellites are assumed to fly in the same orbit with the separation of 10 km along-track-only baseline while flying at the same velocity. It must be noted that the assumed geometry is a simplification based on the actual SAOCOM-CS mission phases.

The swath is illuminated by the MS while the receive-only CS is mechanically steered towards to the desired swath center for Stripmap imaging [7]. Furthermore, the along-track baseline is short enough to create a narrow bistatic angle that results in "quasi-monostatic" geometry [3]. The main parameters are given in Table 1.

3. SAR PERFORMANCE PARAMETERS

3.1. Noise Equivalent Sigma Zero (NESZ)

The monostatic NESZ can be directly derived from the radar equation [4]. In the bistatic configuration, the NESZ is mainly impacted by the longer path and larger incidence angle on the receiver, and it is obtained by replacing the monostatic factor with the factor of the corresponding bistatic configuration [7]:

$$\text{NESZ}_b = \frac{2(4\pi)^3 R_{Tx}^2 R_{Rx}^2 (\sin(\eta_{Tx}) + \sin(\eta_{Rx}))kFT_0 v_r}{P_{av} G_{Tx} G_{Rx} \delta_{sr}(R_{Tx} + R_{Rx})},$$
(1)

where δ_r is the slant range resolution, P_{av} is the average power, λ is the wavelength, k is the Boltzmann's constant, T_0 is the reference temperature, G is the gain, η is the incidence angle, R is the slant range, and the subscripts Tx and Rx denote the transmitter (MS) and the receiver (CS), respectively. Furthermore, v_r is the effective velocity of the satellite and F is the noise factor of the receiver.

3.2. Ambiguities in the Monostatic Case

Range ambiguities are caused by the simultaneous arrival of the reflected echoes from preceding and succeeding pulses outside the desired range region. The range ambiguity to signal ratio (RASR) is given by [4]:

$$\text{RASR}_m = \frac{\sum_{i=1}^{N_{rasr}} S_{a_i}}{\sum_{i=1}^{N_{rasr}} S_i},$$
(2)

where i represents a discrete point in the data record window with a maximum number of time intervals N_{rasr}. S_i is the unambiguous signal power and S_{a_i} is ambiguous signal power that is a function of two-way elevation antenna pattern, backscattering coefficient, the corresponding range vector from platform to the ground range point.
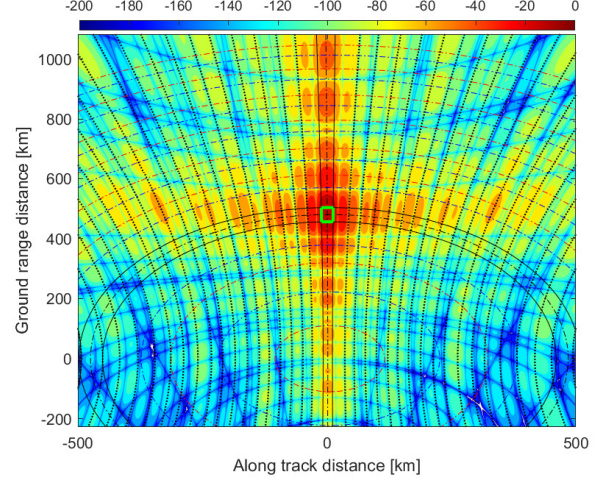

Fig. 1. Plane projected two-way antenna pattern with the bistatic iso-Doppler and iso-range lines. Color scale is in [dB].

Azimuth ambiguity is caused by undersampling the Doppler spectrum. The azimuth ambiguities contributions originate from the Doppler frequency regions outside a frequency support of width PRF centered around f_D, where f_D is the doppler centroid set for the image focusing and PRF the pulse repetition frequency.

The azimuth ambiguity can be quantified by the ratio called azimuth ambiguity to signal ratio (AASR), and the AASR for the monostatic configuration is given by [10]:

$$\text{AASR}_m = \frac{\sum_{k\neq0,k=-N_A}^{N_A} \int_{-B_{dp}}^{+B_{dp}} |C_{2\text{way,az}}(f_D + k \cdot \text{PRF})|^2 \, df}{\int_{-B_{dp}}^{+B_{dp}} |C_{2\text{way,az}}(f_D)|^2 \, df},$$
(3)

where B_{dp} is Doppler bandwidth, $C_{2\text{way,az}}(f_D)$ is the two-way azimuth pattern as a function of the Doppler frequency and N_A is the total number of ambiguities in the calculation.

3.3. Ambiguities in the Bistatic Case

The range and azimuth ambiguities in the bistatic geometry can be derived by projecting the two-way radiation pattern of MS and CS to the ground [7]. The projected pattern for the bistatic configuration of this study is shown in Fig. 1 with the imaged area at a given instant shown as a green box. The black dash-dotted iso-range line crosses the mid-swath of the area of interest and is located in between two black solid iso-range lines that correspond to the near and far range. The black dash-dotted bistatic iso-Doppler line that intersects the mid-swath is bounded between two black solid iso-Doppler lines with a separation of Doppler (processing) bandwidth. The ambiguities are bounded with iso-range and iso-Doppler lines. Further, the bistatic iso-range lines are found by [7]:

5248

$$R_{Txi} + R_{Rxi} = R_{Tx} + R_{Rx} + ic_0/\text{PRF}, \qquad (4)$$

and the bistatic iso-Doppler lines are given by [7]:

$$f_{Db} \cong \frac{1}{\lambda} \left(\frac{\vec{v}_{Tx} \cdot \vec{R}_{Tx}}{R_{Tx}} + \frac{\vec{v}_{Rx} \cdot \vec{R}_{Rx}}{R_{Rx}} \right), \qquad (5)$$

where i denotes considered number of iso-range lines, c_0 is the speed of light, $\vec{R}$ is the slant range vector, R is the norm of the slant range, and v is the velocity vector.

The ambiguous range regions can be calculated by using (4) and two-way near and far slant ranges [7]. The near edge of the range ambiguous region is shown with blue dash-dotted iso-range lines while the far edge with red ones. The range ambiguous regions can be found by summing up the intersection of the range ambiguous regions with the iso-Doppler line that crosses the center of the swath (blue dash-dotted line). The bistatic backscattering coefficient can be approximated as monostatic with quasi-monostatic assumption [3].

The azimuth ambiguities are estimated with a similar approach. The ambiguous regions are computed by using the the corresponding adjacent iso-Doppler lines defining the processed bandwidth, B_{Dp}, which are illustrated with black solid vertical lines in Fig. 1, and the ambiguous iso-Doppler lines which are found by [7]:

$$f_{Dbi} = f_{Db} + iPRF, \qquad |f_{Dbi}| \leq B_{Dp}, \qquad (6)$$

where i denotes the chosen number of ambiguities. The AASR is computed from the bistatic center iso-range cut of the two-way projected pattern and the intersection points of the cut with the ambiguous bistatic iso-Doppler lines given in (6).

4. GENETIC ALGORITHM OPTIMIZER

The joint non-linear problem is solved by exploiting the amplitude-only binary-coded Genetic algorithm (BGA) [5]. The excitation coefficients of the phased arrays are represented as genes. The collection of all genes for a given generation is called a chromosome.

The initial chromosomes of MS and CS are generated randomly, and each chromosome of MS is paired with a random chromosome of CS in the generation of the population. After the evaluation of the fitness function, the fittest individuals become parents of the next generation. These parents are fed to the crossover operation with crossover probability of P_{cross} and the mutation operation with a probability of P_{mut}. The conventional BGA was modified by developing a new swap operator to generate new pairs of MS and CS. This operator takes random chromosomes of MS from the new generation and pairs them with randomly chosen chromosomes of CS to increase the diversity of the candidate solutions. The partial fitness function is calculated by: $F_i = \sum_k^3 w_{i,k} \times \Psi(P_{i,k})$ where i stands for the monostatic and bistatic configurations,

$P_{i,1}$ is the mean of the RASR, $P_{i,2}$ is the AASR, $P_{i,3}$ is the mean NESZ, and w is the weight. Furthermore, a limiting function, Ψ is used to have a dynamic range mapping for the performance metrics. Ψ maps the corresponding performance metric from 0 to 1. For this purpose, a sigmoid function with different offsets and slopes is used for each performance parameter. Finally, the cost function is defined with the weighted sum of the fitness functions of MS and CS: $F_{tot} = w_m \times F_m + w_b \times F_b$ with F_m is the monostatic cost, and F_b is the bistatic cost.

5. RESULTS

The amplitude-only BGA was implemented. Each gene was coded with 6 bits, and the phase coefficients of the MS and CS were pre-calculated considering the radiation pattern electronic steering. The weights of the cost function were experimentally chosen as $w_{i,1} = 0.7$, $w_{i,2} = 0.9$, $w_{i,3} = 1$, $w_m = 0.6$ and $w_b = 1$, which gave good convergence for the current problem. A total of 20 independent realizations were run, each comprising 500 iterations. On each iterations, 40 random chromosome pairs are generated. The best pair is taken as the optimum solution after each realization, and the fittest pair is chosen as the optimum from all the realizations. The performance comparison between the optimized coefficients and the unoptimized coefficients (unit amplitudes) is presented in Table 3.

The results of the RASR vs. ground range at zero Doppler for both monostatic and bistatic configurations are given in Fig. 2. The optimized RASR of the monostatic configuration shows that the range ambiguity is lower and has a smoother behavior along the swath. In Fig. 2(b), the RASR in bistatic configuration is also lower, remaining close to -20 dB for most of the swath. The comparison of the mean RASR values in Table 3 shows a significant performance improvement. Furthermore, Fig. 3(a) and 3(b) illustrate the suppression of the ambiguous range regions for the corresponding cuts.

The optimization result of the AASR is shown in Table 3. The results show that the improvement of the AASR in the monostatic configuration was not significant, which was mainly due to the low number of available array elements in the azimuth direction. Fig. 3(c) shows the two-way normalized azimuth pattern of MS with its ambiguous regions. The suppression of the sidelobes causes a widening of the main beam. As a consequence, more power from the main beam

Selection type	Tournament	Population size	60
Crossover type	Multi-point	Parents	30
P_{cross}	0.8	Swaps	10
P_{mut}	0.2	Iteration	500
Swap type	Random	Realizations	20

Table 2. GA parameters.

	Monostatic		Bistatic	
	Unopt.	**Opt.**	**Unopt.**	**Opt.**
RASR	-27.5 dB	-36.8 dB	-14 dB	-21.2 dB
AASR	-22 dB	-22.1 dB	-13.7 dB	-14.7 dB

Table 3. Optimization results.

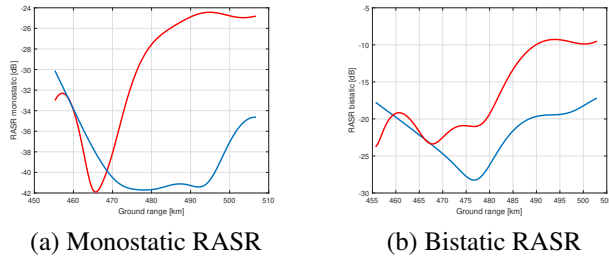(a) Monostatic RASR (b) Bistatic RASR

Fig. 2. Unoptimized (red) and optimized (blue) RASR vs. ground range at zero Doppler.

becomes directed towards the ambiguous region, increasing AASR. Nonetheless, the AASR of the bistatic configuration was improved by 1 dB as shown in Table 3.

The NESZ of the optimized monostatic configuration was below -27 dB along all access range while it was initially below -29 dB. As for the bistatic configuration, the NESZ was initially -21 dB and remained below approximately -20 dB after the optimization.
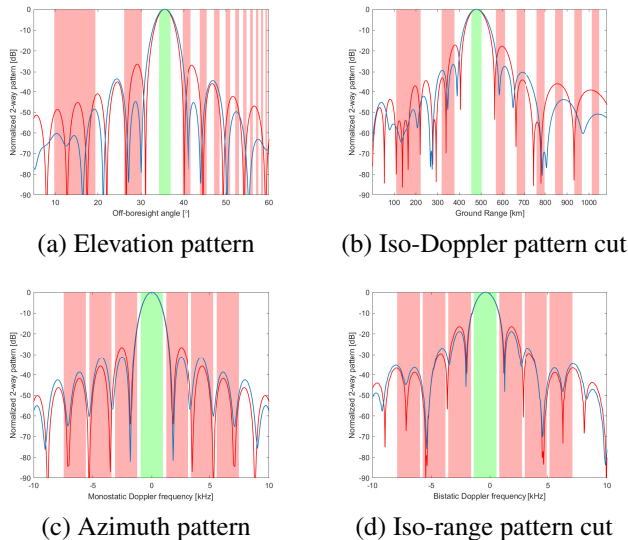

(a) Elevation pattern (b) Iso-Doppler pattern cut

(c) Azimuth pattern (d) Iso-range pattern cut

Fig. 3. Two-way antenna patterns of the monostatic (left) and bistatic (right) configurations with their corresponding ambiguous regions. Red pattern: unoptimized pattern; blue pattern: optimized pattern; red highlight: ambiguous region; green highlight: unambiguous region.

6. CONCLUSION

In this paper, a GA optimizer has been developed to jointly optimize the imaging performance of a simultaneous monostatic and bistatic SAR configuration. The results have shown significant improvements on the ambiguity levels for both configurations.

7. REFERENCES

[1] G. Krieger and A. Moreira, "Spaceborne bi- and multi-static SAR: potential and challenges," *IEE Proc.-Radar Sonar Navig.*, vol. 153, June 2006.

[2] O. Dogan, F. Uysal, and P.L.Dekker, "Unambiguous recovery of multistatic SAR data for nonzero cross track baseline case," *IEEE Geoscience and Remote Sensing Letters*, September 2020.

[3] R. Wang and D. Yunkai, *Bistatic SAR System and Signal Processing Technology*, Springer, 2018.

[4] J.C. Curlander and R.N. McDonough, *Synthetic Aperture Radar Systems and Signal Processing*, John Wiley Sons, 1991.

[5] D. Marcano, "Synthesis of linear and planar antenna arrays using genetic algorithms," *IEEE Antennas and Propagation Society International Symposium*, vol. 3, 1997.

[6] F.J. Villegas, "Parallel genetic-algorithm optimization of shaped beam coverage areas using planar 2-d phased arrays," *IEEE Transactions on Antennas and Propagation*, vol. 55, June 2007.

[7] F. Bordoni, M. Younis, M. Rodriguez-Cassola, P. Prats-Iraola, P. López-Dekker, and G. Krieger, "SAOCOM-CS sar imaging performance evaluation in large baseline bistatic configuration," *Proc. of IEEE Int. Geoscience and Remote Sensing Symposium (IGARRS)*, 2015.

[8] N. Gebert, B.C. Domínguez, M.W.J. Davidson, M.D. Martin, and P. Silvestrin, "SAOCOM-CS – a passive companion to SAOCOM for single-pass l-band sar interferometry," *Proc. of 10th European Conference on Synthetic Aperture Radar*, 2014.

[9] D. D'Aria, D. Giudici, A. Monti-Guarnieri, P. Rizzoli, and J. Medina, "A wide swath, full polarimetric, l-band spaceborne SAR," *Proc. of Radar Conference, Roma, IT*, May 2008.

[10] M. Younis et al., "Performance comparison of reflector- and planar-antenna based digital beam-forming SAR," *International Journal of Antennas and Propagation*, pp. 1–13, 2009.